ACS Macro Letters

Letter

pubs.acs.org/macroletters

Self-Propelled Microswimmer Actuated by Stimuli-Sensitive Bilayered Hydrogel

Svetoslav V. Nikolov, Peter D. Yeh, and Alexander Alexeev*

George W. Woodruff School of Mechanical Engineering, Georgia Institute of Technology, Atlanta, Georgia 30332-0405, United States

Supporting Information

ABSTRACT: Using computational modeling, we design a microscopic swimmer made of a bilayered responsive hydrogel capable of swimming in a viscous fluid when actuated by a periodically applied stimulus. The gel has an X-shaped geometry and two bonded layers, one of which is responsive to environmental changes and the other which is passive. When the stimulus is turned on, the responsive layer swells and causes the swimmer to deform. We demonstrate that when such stimulus-induced deformations occur periodically the gel swimmer effectively propels forward through the fluid. We show that the swimming speed depends on the relative stiffness of the two gel layers composing the swimmer, and we determine the optimal stiffness ratio that maximizes the swimming speed.

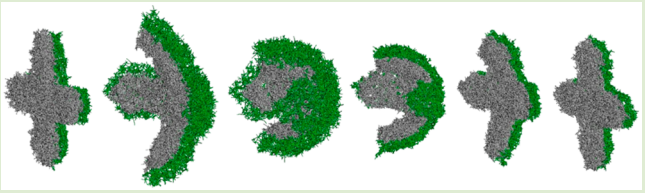

As robotic swimmers become ever smaller and approach the microscale realm, researchers have developed a variety of clever methods to generate propulsion of miniature objects submerged in an aqueous solution. Such microscale swimmers could use biocatalytic propulsors, biomimetic nanowires that beat like synthetic flagella, responsive soft materials, and other approaches to propel themselves through a viscous fluid.[1−9] Further advances in microswimmer development could yield highly maneuverable and controllable robots that can be targeted to specific locations and autonomously perform complex tasks[10−13] and therefore can be effectively utilized in such applications as drug delivery, biosensing, micromanufacturing, and microsurgery.[14−19]

A critical requirement of synthetic microswimmers is their ability to generate self-propelling motion in a fluid environment dominated by viscous forces without using complex mechanical machinery employed by larger macroscopic swimming devices. In this respect, soft responsive hydrogels that are typically biocompatible are especially attractive for designing active microscopic devices. Responsive hydrogels can generate a large amplitude mechanical motion controlled by chemical reactions[20,21] or in response to various external environmental changes[22,23] that include changes in temperature, pH, electric and magnetic fields, and light.[24−27] In other words, the motion of hydrogel swimmers can be directly controlled by changing their environment. The response time of hydrogels depends on the diffusion rate of the solvent into the swelling gel network and is proportional to the squared size of the network. Thus, micrometer-sized gels can exhibit response times on the order of seconds[28,29] and even faster,[30,31] similar to fast switching liquid-crystal elastomers,[32,33] which makes these materials suitable for applications requiring rapid periodical actuation.

In our study, we use computational modeling to design an efficient autonomous microswimmer that is actuated using a responsive hydrogel and features a simple, easy-to-implement design. Our simulations show that an on/off periodic application of an external stimulus on the gel swimmer can lead to a rapid self-propelled motion caused by periodic swimmer deformations. More specifically, our gel microswimmer is made of a bifacial hydrogel sheet consisting of two thin gel layers that are bonded together. One layer with thickness d_R swells in response to an external stimulus, whereas the second layer is nonresponsive and has a thickness d_P (Figure 1a). Except for stimuli sensitivity, both layers are characterized by identical material properties.

When the bilayered Janus-like gel sheet is exposed to an appropriate stimulus, the initially flat and stress-free material undergoes simultaneous expansion and bending. The responsive layer expands, effectively increasing the lateral size of the gel sheet. At the same time, a mismatch between stresses develops in the responsive and passive layers, resulting in an internal bending moment. The bilayered gel sheet thus bends out-of-plane to equilibrate these stresses.

As presented in Figure 1b, we adopt an X-shaped geometry for the gel swimmer with equal height and width dimensions, represented by body length L. With this configuration, four swimmer arms bend toward the swimmer center when a stimulus is imposed. Upon removal of the external stimulus the swimmer straightens back to the original configuration, assuming its initially flat shape. As we show below, this simple microswimmer made of bifacial hydrogel can effectively self-propel in a highly viscous fluid environment when actuated by a periodically applied external stimulus.

We model the responsive polymer gel as a network of interconnected elastic filaments.[34,35] To investigate the hydro-

Received: November 3, 2014
Accepted: December 22, 2014
Published: December 26, 2014

DOI: 10.1021/mz5007014
ACS Macro Lett. 2015, 4, 84−88

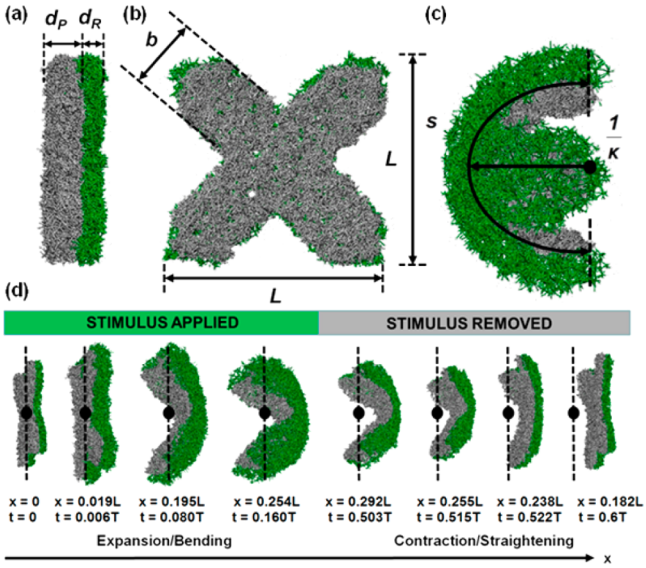

Figure 1. Microswimmer made of a bifaced hydrogel. (a) The gel swimmer has two layers: a responsive layer (green) and passive layer (gray) with thicknesses d_R and d_P, respectively. The responsive layer swells and expands when an appropriate external stimulus is applied. (b) Front view of the X-shaped gel swimmer. The swimmer body has length L, and its arms have width b. (c) The swimmer expands and bends in response to an external stimulus. Its deformation is characterized by curvature κ and arc length s. (d) Simulation snapshots of the microswimmer during one period of its motion. The swimmer propels in the positive x direction. The dotted lines indicate the initial x position of the swimmer's center of mass (solid circle) at $t = 0$. When the stimulus is applied at $t = 0$ the swimmer expands and bends. When the stimulus is removed at $t = 0.5T$, the swimmer contracts and straightens to its original configuration.

dynamics of this gel swimmer in a viscous Newtonian solvent, we employ dissipative particle dynamics (DPD).[36−38] Briefly, DPD is a coarse-grained technique in which clusters of molecules are represented by beads that interact via "soft" pairwise potentials. The use of soft potentials makes it possible to simulate dynamics of polymeric systems on relatively large time and space scales. Moreover, the pairwise potentials are momentum conservative thereby allowing for hydrodynamic simulations with even a relatively small number of beads. The details of our computational methodology can be found in the Supporting Information.

In our simulations we actuate the swimmer by applying an external stimulus with a period T. The stimulus is applied during the first half of the period and is turned off during the latter half. As a result, the swimmer exhibits periodical shape changes as illustrated in Figure 1d. When the stimulus is applied at $t = 0$ and the responsive layer swells, the swimmer rapidly expands by increasing the length of the arms. The swimmer expansion is complemented by a slow bending of the arms, which continues until the swimmer equilibrates at the bended state. After that, the shape remains unchanged until the stimulus is removed at $t = 0.5T$. From this time until the end of the period, the responsive layer deswells, and the swimmer recovers its initial flat shape. This recovery process includes rapid contraction of the arms complemented by their relatively slow straightening. This sequence of geometrical shape changes repeats after the stimulus cycle is reapplied and leads to a forward motion of the swimmer.

To characterize the forward motion of our gel swimmer in a viscous fluid, we tracked the position of the swimmer's center of mass as it moved. Figure 2a shows this position in the

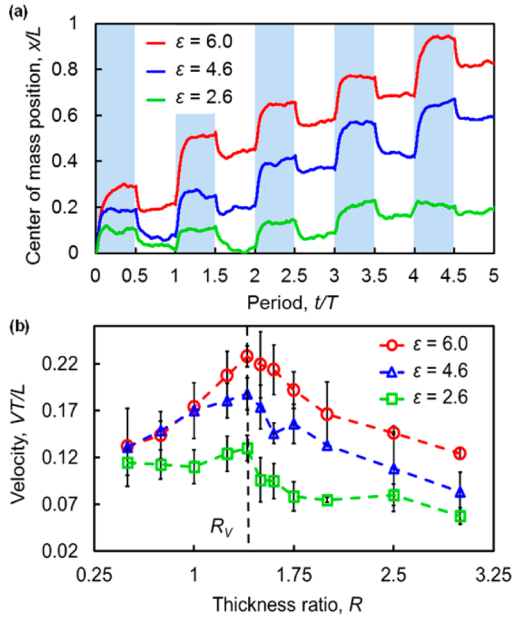

Figure 2. (a) Center of mass position vs period for different swelling ratios of the swimmer's responsive gel layer. Colored background indicates the portion of time when the stimulus is on. During one period, the swimmer undergoes bending and expansion, moving forward after the stimulus application. Upon stimulus removal, the swimmer undergoes contraction and straightening and moves backward a shorter distance. The result is a net forward displacement. (b) Swimming velocity V as a function of thickness ratio $R = d_P/d_R$. Error bars indicate standard deviation from the average value. The optimal thickness ratio $R_V = 1.4$ leading to the fastest swimming speed is indicated by the vertical dashed line.

direction of the swimmer motion as a function of time. In this figure we normalized the swimmer's displacement x by the initial body length L and the time by the swelling period T. We find that the swimmer can rapidly propel itself forward in the positive x direction. Analysis of the swimmer's trajectory indicates that the swimmer swelling and deswelling produce, respectively, forward and backward strokes. When the stimulus is applied and the gel swells, the center of mass moves forward until the swimmer equilibrates at a new position. Gel deswelling associated with stimulus removal causes the center of mass to move backward. During the backward stroke, however, the swimmer's displacement is smaller than during the forward stroke, thereby yielding a net forward displacement of the swimmer's body over one period.

We find that the swimmer moves forward faster when the swelling ratio of the responsive gel layer $\varepsilon = V_s/V_c$ is increased (Figure 2a). Here, V_c and V_s are, respectively, the volumes of an unconstrained responsive gel before and after the stimulus is applied. A larger swelling ratio amplifies the swimmer's deformation and therefore leads to faster swimming. In addition to the swelling ratio, the motion of our simple X-shaped gel microswimmer is defined by the relative elasticity of the passive and responsive layers. In our simulations we change the thickness of the passive gel layer d_P while keeping constant the thickness of the responsive layer d_R. Since the stiffness of individual network filaments in both gel layers is identical,

DOI: 10.1021/mz5007014
ACS Macro Lett. 2015, 4, 84−88

changing d_P allows us to alter the stiffness ratio between the two layers.

The average propulsion velocity of the swimmer is summarized in Figure 2b where the velocity V, normalized by L/T, is shown as a function of the swimmer's thickness ratio $R = d_P/d_R$ for three selected values of ε. Here, we find that increasing ε systematically increases the swimmer's velocity. However, the dependence on the thickness ratio R is not monotonic. The velocity decreases when the thickness of the passive layer is either too small or too large and is maximized for all values of ε when the thickness ratio is about 1.4. The velocity maximum is most pronounced for the larger swelling ratio $\varepsilon = 6$, in which case it is equal to 0.22 body lengths per period. In other words, this swimmer travels a distance equal to its body length in only about four stimulus cycles. Such a fast propulsion speed is quite remarkable for microscopic systems moving in a highly viscous fluid. In fact, this swimming speed is comparable to that of *E. coli*, which uses about four to five beating cycles to move one body length.[39]

Due to its small size, the dynamics of the swimmer is dominated by viscous forces. In this case, a time irreversible stroke is required to propel forward.[40] To examine the physics governing the microswimmer motion in its inertialess environment, we introduce two parameters that characterize the swimmer shape (see Figure 1c). Specifically, we use the arc length s that represents the extent of the swimmer arms and the swimmer curvature κ that characterizes the magnitude of bending. Figure 3a shows how these parameters (normalized by the initial length L of the swimmer) change in time when the gel swimmer undergoes periodic swelling and deswelling. When the stimulus is applied, the gel swimmer expands laterally and bends as indicated by the increasing values of the arc length s and curvature κ. Upon deswelling of the responsive layer, the arm length decreases, and the swimmer straightens to nearly zero curvature. In our simulations, we set the stimulus application period T to be much longer than the swelling time. For the conditions in Figure 3, the changes in s and κ occur within about 5% of T immediately after the stimulus is applied or removed, whereas during the rest of the actuation cycle, s and κ remain nearly constant, showing slight changes induced by thermal fluctuations.

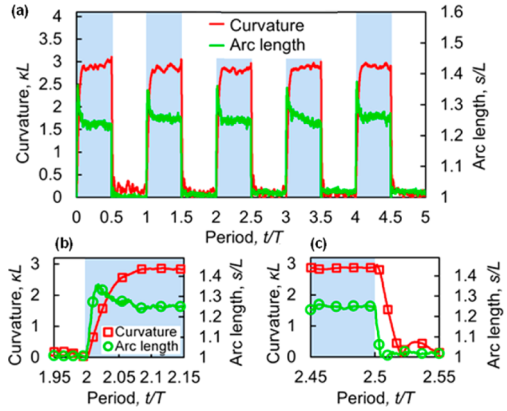

Figure 3. Swimmer deformation due to periodic application of the stimulus. Colored background indicates portion of time when stimulus is on. (a) Arc length and curvature vs time for the microswimmer with $R = 1.5$ and $\varepsilon = 6$. The arc length and curvature rapidly increase to a new equilibrium state after the stimulus is applied and then revert back to their original states upon stimulus removal. The time scale difference between rates of change in arc length and curvature is illustrated during (b) swelling and (c) deswelling. In both cases, changes in arc length occur more quickly than that of curvature. This results in a time-irreversible motion that yields propulsion in a highly viscous environment.

Figure 3b and 3c shows the evolution of s and κ at moments when the stimulus state is changed. The figures indicate that changes of the swimmer's arc length occur substantially faster than changes of the swimmer's curvature. Thus, the swimmer motion can be approximated by four sequential steps. When the stimulus is applied, the swimmer first extends the arms and then bends. After the stimulus is removed, the arms contract and then straighten. As a consequence of this cyclic motion, the swimmer's arm length is greater during bending (forward stroke) than during straightening (backward stroke), thus yielding the required time-irreversible motion. In other words, the mismatch in time scales associated with swimmer stretching and bending allows the bilayered swimmer to move forward throughout a highly viscous environment.

The bending and stretching time scales, t_b and t_e, can be estimated using a scaling analysis of the swimmer motion whose details are presented in the Supporting Information. The scaling indicates that $(t_e/t_b) \sim (C_e/C_b)[(8(1 + R\varepsilon^{-1/3})^3)/(3R\varepsilon^{-1/3})](d_R/L)^2$. Thus, the time ratio depends on the ratio of the drag coefficients for swimmer extension and bending $C_e/C_b \sim 0.5$,[41] the swimmer aspect ratio d_R/L that is defined by the swimmer geometry, and $R\varepsilon^{-1/3}$, the thickness ratio of the swollen swimmer. Note that there is no dependence on material properties other than the swelling ratio ε. Time-irreversible motion emerges when $t_e/t_b \ll 1$ in which case the aspect ratio d_R/L should be small and the swollen thickness ratio $R\varepsilon^{-1/3}$ should be about 0.5. Furthermore, our scaling analysis predicts the swimmer length in the swollen state as $s_{max}/L \sim (\varepsilon^{1/3} + R)/(1 + R)$ and maximum curvature $\kappa_{max}L \sim [(6R(1 - \varepsilon^{-1/3}))/(\varepsilon^{1/3}(1 + R\varepsilon^{-1/3}))](L/d_R)$.

In Figure 4, we plot the magnitudes of the maximum extent of swimmer stretching s_{max} and bending κ_{max} in one swimming cycle obtained in our simulations and compare them to the predictions of the scaling model. The simulations and the model yield similar trends. In particular, the maximum swimmer extension s_{max} steadily decreases with increasing R. Moreover, when R increases, the swollen length ratio decreases and approaches unity, meaning that the swimmer with large R is unable to expand due to larger resistance of the passive layer.

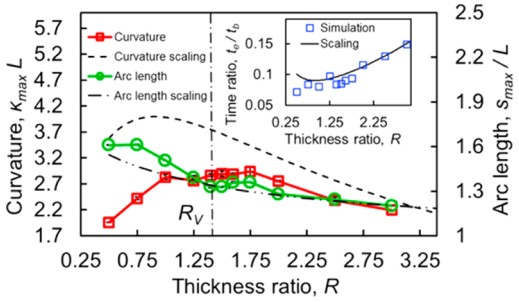

Figure 4. Maximum curvature, maximum arc length, and ratio between expansion and bending times (inset) as a function of thickness ratio. Dark lines indicate corresponding scaling arguments. Simulation data exhibit the same trends as predicted by scaling. The maximum swimming speed occurs in the range of thickness ratios for which the curvature is maximized, whereas the time ratio is minimized.

DOI: 10.1021/mz5007014
ACS Macro Lett. 2015, 4, 84−88

The scaling model predicts a maximum for κ_{max}, which appears in the simulations as a plateau between $R = 1$ and $R = 2$. When R is either larger or smaller, the curvature decreases indicating that the swimmer does not bend. Indeed, for small R, the thin passive layer is unable to resist the expansion, generating a weak internal bending moment. For large R, the thick passive layer suppresses the bending of the swimmer. Furthermore, we find that the scaling model and simulations predict that the ratio of time scales between stretching and bending, t_e/t_b, has a minimum at $R \sim 1$ (see the inset in Figure 4).

By comparing Figures 2b and 4, we notice that R_V characterizing the fastest swimmer propulsion lies nearly in the middle of the range where the swimmer curvature is maximized. This result indicates that the increased swimmer bending enhances the swimmer's velocity because in this case the swimmer's forward stroke can displace fluid farther. In addition to bending, the swimming speed is enhanced by larger arm extension between the forward and backward strokes. The amount of this extension, $\Delta s = s_{max} - L$, is proportional to the net amount of solvent displaced during the swimmer stroke. However, without sufficient bending a greater Δs does not result in faster swimming. Indeed, for small R the velocity drops due to the lack of bending as indicated by a reduced κ_{max}. Thus, the fastest swimmer is achieved with an optimal combination of arc length and curvature changes in which neither parameter is too small.

One of the major advantages of our swimmer is that it can be experimentally implemented using a variety of bilayered polymeric materials. In fact, bilayered swimmers could have different shapes, elasticity of layers, and stimuli-induced responsiveness provided that they yield relatively large magnitudes of stretching and bending deformations. The time ratio of these deformations must be relatively small, and the velocity must satisfy the low-Reynolds number hydrodynamics. In other words, our swimmer design allows for a variety of experimental realizations that could involve a broad class of polymeric materials. Indeed, ongoing developments in designing actuating bilayered responsive gels offer a number of materials that demonstrate large amplitude deformation response to external stimuli[7,32,33,42−47] that could be potentially used to build our gel swimmer. Furthermore, several groups have successfully demonstrated ground locomotion ("walkers" or "jumpers") using responsive gels, further emphasizing the utility of these materials in soft robotic applications.[7,22,42,48] We note that the systems in these studies are on the order of hundreds of microns, a relatively large scale, whereas our gel swimmer design is directly applicable to micrometer-sized and even smaller systems. Recent progress in synthesizing bilayered gels shows promise in downscaling such responsive materials to micrometer and nanometer scales.[49] For example, recombinant DNA (rDNA) technology is a promising method that can be utilized to synthesize micrometer sized gels with accurately controlled molecular architecture. Through this approach researchers were able to generate film assemblies as thin as 100 nm.[50]

In summary, we used computer simulations to design a self-propelling gel microswimmer actuated by a periodically applied external stimulus that can move unidirectionally in a fluid environment dominated by viscous forces. Our simple swimmer establishes design principles for developing more sophisticated swimmers that can be enriched with additional functions and capabilities. For example, adding extra responsive sections may be employed for directing the swimmer in three dimensions and controlling its turning.[10] Using binding molecules at the front, our swimmer could be potentially used for uploading and transporting different microscopic cargo.[51] Finally, since external stimuli can simultaneously actuate multiple independent gel swimmers, a swarm of such microscopic devices could be harnessed to accomplish tasks that are unachievable for a single microswimmer. Future computational studies and experiments are therefore needed to explore these exciting research paths.

■ ASSOCIATED CONTENT

Supporting Information

(1) Description of the computational methodology and description of the scaling analysis. (2) Animations of the hydrogel actuated microswimmer in motion with thickness ratio $R = 1.4$ and swelling ratio $\varepsilon = 6$. This material is available free of charge via the Internet at http://pubs.acs.org.

■ AUTHOR INFORMATION

Corresponding Author

*E-mail: alexander.alexeev@me.gatech.edu.

Author Contributions

The manuscript was written through contributions of all authors. All authors have given approval to the final version of the manuscript.

Notes

The authors declare no competing financial interest.

■ ACKNOWLEDGMENTS

Financial support by NSF CAREER Award DMR-1255288 and helpful discussions with V. V. Tsukruk are gratefully acknowledged.

■ REFERENCES

(1) Roper, M.; Dreyfus, R.; Baudry, J.; Fermigier, M.; Bibette, J.; Stone, H. A. *Proc. R. Soc. A* **2008**, *464*, 877−904.

(2) Dreyfus, R.; Baudry, J.; Roper, M. L.; Fermigier, M.; Stone, H. A.; Bibette, J. *Nature* **2005**, *437*, 862−865.

(3) Gao, W.; Peng, X. M.; Pei, A.; Kane, C. R.; Tam, R.; Hennessy, C.; Wang, J. *Nano Lett.* **2014**, *14*, 305−310.

(4) Lin, C. T.; Kao, M. T.; Kurabayashi, K.; Meyhöfer, E. *Small* **2006**, *2*, 281−287.

(5) Wang, J.; Gao, W. *ACS Nano* **2012**, *6*, 5745−5751.

(6) Hess, H. *Annu. Rev. Biomed. Eng.* **2011**, *13*, 429−450.

(7) Geryak, R.; Tsukruk, V. V. *Soft Matter* **2014**, *10*, 1246−1263.

(8) Golestanian, R.; Liverpool, T. B.; Ajdari, A. *New J. Phys.* **2007**, *9*, 126.

(9) Qiu, T.; Lee, T.-C.; Mark, A. G.; Morozov, K. I.; Münster, R.; Mierka, O.; Turek, S.; Leshansky, A. M.; Fischer, P. *Nat. Commun.* **2014**, *5*, 5119.

(10) Masoud, H.; Bingham, B. I.; Alexeev, A. *Soft Matter* **2012**, *8*, 8944−8951.

(11) Ebbens, S. J.; Buxton, G. A.; Alexeev, A.; Sadeghi, A.; Howse, J. R. *Soft Matter* **2012**, *8*, 3077−3082.

(12) Weibel, D. B.; Garstecki, P.; Ryan, D.; Diluzio, W. R.; Mayer, M.; Seto, J. E.; Whitesides, G. M. *Proc. Natl. Acad. Sci. U.S.A.* **2005**, *102*, 11963−11967.

(13) Zhang, L.; Petit, T.; Lu, Y.; Kratochvil, B. E.; Peyer, K. E.; Pei, R.; Lou, J.; Nelson, B. J. *ACS Nano* **2010**, *4*, 6228−6234.

(14) Hu, J.; Liu, S. *Macromolecules* **2010**, *43*, 8315−8330.

(15) Döring, A.; Birnbaum, W.; Kuckling, D. *Chem. Soc. Rev.* **2013**, *42*, 7391−7420.

(16) Deligkaris, K.; Tadele, T. S.; Olthuis, W.; van den Berg, A. *Sens. Actuators, B* **2010**, *147*, 765−774.

DOI: 10.1021/mz5007014
ACS Macro Lett. 2015, 4, 84−88

(17) Stuart, M. A. C.; Huck, W. T.; Genzer, J.; Müller, M.; Ober, C.; Stamm, M.; Sukhorukov, G. B.; Szleifer, I.; Tsukruk, V. V.; Urban, M. *Nat. Mater.* **2010**, *9*, 101−113.
(18) Smeets, N.; Hoare, T. *J. Polym. Sci., Part A: Polym. Chem.* **2013**, *51*, 3027−3043.
(19) Mano, J. F. *Adv. Eng. Mater.* **2008**, *10*, 515−527.
(20) Yoshida, R.; Ueki, T. *NPG Asia Mater.* **2014**, 6.
(21) Yashin, V. V.; Balazs, A. C. *Science* **2006**, *314*, 798−801.
(22) Morales, D.; Palleau, E.; Dickey, M. D.; Velev, O. D. *Soft Matter.* **2014**, *10*, 1337−1348.
(23) Osada, Y.; Gong, J. P. *Prog. Polym. Sci.* **1993**, *18*, 187−226.
(24) Zrinyi, M. *Colloid Polym. Sci.* **2000**, *278*, 98−103.
(25) Roy, D.; Cambre, J. N.; Sumerlin, B. S. *Prog. Polym. Sci.* **2010**, *35*, 278−301.
(26) Ahn, S.-K.; Kasi, R. M.; Kim, S.-C.; Sharma, N.; Zhou, Y. *Soft Matter* **2008**, *4*, 1151−1157.
(27) Filipcsei, G.; Feher, J.; Zrínyi, M. *J. Mol. Struct.* **2000**, *554*, 109−117.
(28) Beebe, D. J.; Moore, J. S.; Bauer, J. M.; Yu, Q.; Liu, R. H.; Devadoss, C.; Jo, B.-H. *Nature* **2000**, *404*, 588−590.
(29) Xia, L.-W.; Xie, R.; Ju, X.-J.; Wang, W.; Chen, Q.; Chu, L.-Y. *Nat. Commun.* **2013**, *4*, 2226.
(30) Kwon, G. H.; Jeong, G. S.; Park, J. Y.; Moon, J. H.; Lee, S.-H. *Lab Chip* **2011**, *11*, 2910−2915.
(31) Kim, J.; Serpe, M. J.; Lyon, L. A. *Angew. Chem.* **2005**, *117*, 1357−1360.
(32) Camacho-Lopez, M.; Finkelmann, H.; Palffy-Muhoray, P.; Shelley, M. *Nat. Mater.* **2004**, *3*, 307−310.
(33) White, T. J.; Serak, S. V.; Tabiryan, N. V.; Vaia, R. A.; Bunning, T. J. *J. Mater. Chem.* **2009**, *19*, 1080−1085.
(34) Masoud, H.; Alexeev, A. *ACS Nano* **2011**, *6*, 212−219.
(35) Masoud, H.; Alexeev, A. *Macromolecules* **2010**, *43*, 10117−10122.
(36) Groot, R. D.; Warren, P. B. *J. Chem. Phys.* **1997**, *107*, 4423−4435.
(37) Hoogerbrugge, P.; Koelman, J. *Europhys. Lett.* **1992**, *19*, 155−160.
(38) Mills, Z. G.; Mao, W.; Alexeev, A. *Trends Biotechnol.* **2013**, *31*, 426−434.
(39) Chattopadhyay, S.; Moldovan, R.; Yeung, C.; Wu, X. *Proc. Natl. Acad. Sci. U.S.A.* **2006**, *103*, 13712−13717.
(40) Purcell, E. M. *Am. J. Phys.* **1977**, *45*, 3−11.
(41) Cox, R. *J. Fluid Mech.* **1970**, *44*, 791−810.
(42) Ionov, L. *Mater. Today* **2014**, DOI: 10.1016/j.mattod.2014.07.002.
(43) Li, W.; Huang, G.; Yan, H.; Wang, J.; Yu, Y.; Hu, X.; Wu, X.; Mei, Y. *Soft Matter* **2012**, *8*, 7103−7107.
(44) Stoychev, G.; Zakharchenko, S.; Turcaud, S. b.; Dunlop, J. W.; Ionov, L. *ACS Nano* **2012**, *6*, 3925−3934.
(45) Dai, M.; Picot, O. T.; Verjans, J. M.; de Haan, L. T.; Schenning, A. P.; Peijs, T.; Bastiaansen, C. W. *ACS Appl. Mater. Interfaces* **2013**, *5*, 4945−4950.
(46) Wen, H.; Zhang, W.; Weng, Y.; Hu, Z. *RSC Adv.* **2014**, *4*, 11776−11781.
(47) Ji, M.; Jiang, N.; Chang, J.; Sun, J. *Adv. Funct. Mater.* **2014**, *24*, 5412−5419.
(48) Maeda, S.; Hara, Y.; Sakai, T.; Yoshida, R.; Hashimoto, S. *Adv. Mater.* **2007**, *19*, 3480−3484.
(49) Tsukruk, V. V.; Alexeev, A. Compliant and Reconfigurable Nanocomposites: Fabrication, Testing, and Simulations. In *2013 MRS Fall Meeting*, Boston, MA, 2013.
(50) Krishnaji, S. T.; Huang, W.; Rabotyagova, O.; Kharlampieva, E.; Choi, I.; Tsukruk, V. V.; Naik, R.; Cebe, P.; Kaplan, D. L. *Langmuir* **2011**, *27*, 1000−1008.
(51) Wang, J. *Lab Chip* **2012**, *12*, 1944−1950.

DOI: 10.1021/mz5007014
ACS Macro Lett. 2015, 4, 84−88